NANO LETTERS

pubs.acs.org/NanoLett

Letter

A Microcolumn DC Graphene Sensor for Rapid, Sensitive, and Universal Chemical Vapor Detection

Wenzhe Zang, Zhe Liu, Girish S. Kulkarni, Hongbo Zhu, You Wu, Kyunghoon Lee, Maxwell Wei-Hao Li, Xudong Fan,* and Zhaohui Zhong*

Cite This: *Nano Lett.* 2021, 21, 10301−10308

Read Online

ACCESS | Metrics & More | Article Recommendations | Supporting Information

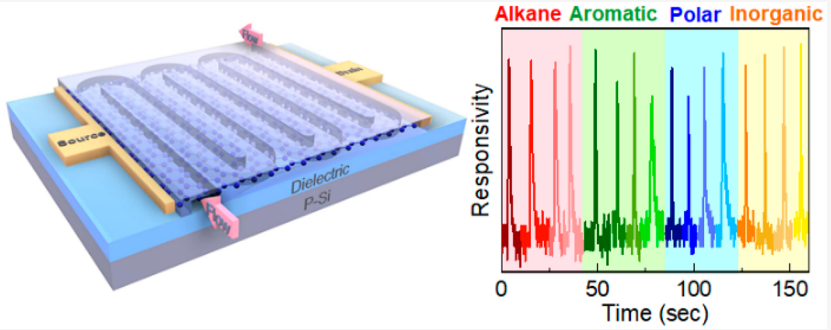

ABSTRACT: Nearly all existing direct current (DC) chemical vapor sensing methodologies are based on charge transfer between sensor and adsorbed molecules. However, the high binding energy at the charge-trapped sites, which is critical for high sensitivity, significantly slows sensors' responses and makes the detection of nonpolar molecules difficult. Herein, by exploiting the incomplete screening effect of graphene, we demonstrate a DC graphene electronic sensor for rapid (subsecond) and sensitive (ppb) detection of a broad range of vapor analytes, including polar, nonpolar, organic, and inorganic molecules. Molecular adsorption induced capacitance change in the graphene transistor is revealed to be the main sensing mechanism. A novel sensor design, which integrates a centimeter-scale graphene transistor and a microfabricated flow column, is pioneered to enhance the fringing capacitive gating effect. Our work provides an avenue for a broad spectrum real-time gas sensing technology and serves as an ideal testbed for probing molecular physisorption on graphene.

KEYWORDS: *Chemical vapor sensing, Graphene, Direct current detection, Fringing capacitive gating effect, Binding energy*

Nanoelectronic sensors based on low dimensional materials benefit from their extremely high surface-to-volume ratio, low power consumption, chemical robustness, and convenient electrical readout. They represent an important emerging technology that potentially has a broad range of applications in environmental protection, industrial safety, and biomedicine.[1−7] Particularly, graphene stands out with its high carrier mobility and compatibility with existing semiconductor fabrication technologies that can be explored for developing on-chip sensitive nanoelectronic sensors with large intrinsic gain.[2,3,8,9]

In a typical nanoelectronic vapor sensor, molecules adsorbed to the sensor surface modify its electronic properties, thus generating the sensing signal. Chemical sensors using the field effect transistor (FET) design stand out due to their high sensitivity, resulting from the intrinsic gain from the electrostatic gating effect. The current voltage relation for an FET-based sensor can be generally expressed as

$$I = \frac{\mu W}{L} C_g \left(V_g - V_{th} - \frac{1}{2} V_{sd} \right) \cdot V_{sd} \quad (1)$$

where μ is the charge carrier mobility, W and L are the channel width and length, respectively, C_g is the gate capacitance, V_g is the gate voltage, V_{sd} is the source−drain bias voltage, V_{th} is threshold voltage, and $C_g(V_g - V_{th} - \frac{1}{2}V_{sd})$ gives the charge per unit area within the FET channel induced by the gate voltage.

Most nanoelectronic chemical sensors exploit the charge transfer between the absorbed analyte molecules and the sensor,[10−16] directly via the nanomaterial or indirectly via the contact metal. Additional charges to the FET channel thus contribute to the total transistor current:

Received: September 2, 2021
Revised: December 3, 2021
Published: December 8, 2021

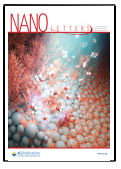

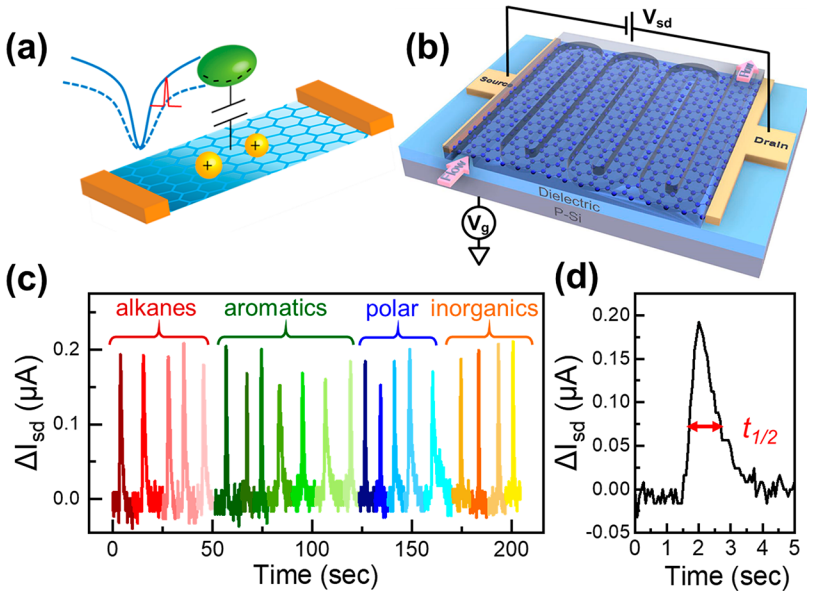

Figure 1. μColumn graphene sensor for universal, rapid, and sensitive chemical vapor detection. (a) Illustration of the fringing capacitance change based sensing mechanism. Fringing capacitive gating occurs when a vapor molecule alters the local electrostatic potential around the graphene channel, which pulls more charges from the metal contacts. The analyte gating effect increases the transconductance of the FET by coupling with the back gate, which can be further amplified by graphene's large mobility and measured conveniently as a DC current change. (b) Schematic showing a Gr-FET covered with a μColumn with a dimension of 40 cm (length) × 400 μm (width) × 370 μm (depth) for enhancing the interaction between vapor analytes and graphene. All analyte sensing tests were conducted with V_g = 0 V and V_{sd} = 3 V unless stated otherwise. The DC current between the source and the drain was recorded as the sensing signal. (c) DC current responses of μColumn graphene sensor to injections of various masses of four groups of analytes, namely, normal alkanes (left to right: C_5−C_9), aromatics (left to right: benzene, toluene, ethylbenzene, *o*-xylene, *m*-xylene, *p*-xylene, chlorobenzene), organic polar compounds (left to right: acetone, chloroform, ethanol, DMF, DMMP), and inorganics (left to right: carbon monoxide, carbon dioxide, nitric oxide, and hydrogen sulfide). (d) Temporal response to heptane with the full width at half-maximum $t_{1/2}$ = 0.6 s (labeled in red arrow).

$$I_{sensor} = \frac{\mu W}{L}\left[C_g\left(V_g - V_{th} - \frac{1}{2}V_{sd}\right) + Q_{mol}\right]V_{sd} \quad (2)$$

where Q_{mol} is the charge transfer between the device and molecules per unit area inside the channel. Therefore, depending on whether the adsorbed molecules are electron donors or acceptors, the changes in the detected current signal can give opposite signs. Such charge transfer behavior tends to happen for molecules with high binding energy to the sensor surface, or at low absorption energy sites resulting from defects.[16] However, slow defect-mediated charge-transfer processes significantly limit those sensors' responses to tens to hundreds of seconds. Additionally, most weak polar and nonpolar molecules are inherently weak charge donors or acceptors, which further limits the utility of the charge transfer mechanism. Alternatively, analyte binding induced changes in carrier mobility have also been explored for sensing. Previous research has intentionally introduced more defects or functional groups to enhance coulomb scattering and lower sensor mobility.[17,18] Under the framework of this mechanism, all the analytes would consistently give negative current changes. Even though in principle this approach can detect both polar and nonpolar molecules, it generally has low sensitivity.

There are also other limitations to the aforementioned two mechanisms. For example, chemo-selective coating or functionalization[18−21] is often required to increase the sensitivity; post-treatments such as vacuum degassing,[13] prolonged heating,[12,22] and ultraviolet radiation[23] are often needed for baseline regeneration. The resulting sensors are impractical for robust on-site vapor monitoring systems, which require rapid real-time responses at low concentrations and fast sensor regeneration.[24,25] Hence, novel sensing mechanisms are needed to resolve these fundamental bottlenecks (*i.e.*, the trade-offs between sensitivity and response time) and take full advantages of nanoelectronic sensors.

Recently, using the intrinsic nonlinearity of a transistor, our groups have pioneered a new sensing technology based on heterodyne mixing to investigate the interaction between the alternating current (AC) drive voltage and the induced oscillating molecular dipole moment.[26−30] By detecting the molecular dipole instead of charge, our heterodyne sensor successfully addresses the fundamental speed-sensitivity trade-off in vapor detection.[28,30] Despite these achievements, this heterodyne sensor cannot detect nonpolar molecules due to its intrinsic dipole moment sensing mechanism; the AC mixing instrumentation is also more complex than traditional DC based circuitry.

This work reports a fringing capacitance change based sensing mechanism by exploiting the incomplete screening of graphene.[31] Unlike sensors made of metals or bulk semiconductors, the binding of molecules on the surface of graphene leads to changes in the gate capacitance of a graphene FET, resulting in current

$$I = \frac{\mu W}{L}(C_g + C_{mol})\cdot\left(V_g - V_{th} - \frac{1}{2}V_{sd}\right)\cdot V_{sd} = \frac{\mu W}{L}\left[C_g\left(V_g - V_{th} - \frac{1}{2}V_{sd}\right) + Q_{mol}\right]V_{sd} \quad (3)$$

where C_{mol} and Q_{mol} are the molecule induced fringing capacitance change and corresponding charge perturbation, respectively. As shown in Figure 1a, fringing capacitance

https://doi.org/10.1021/acs.nanolett.1c03416
Nano Lett. 2021, 21, 10301−10308

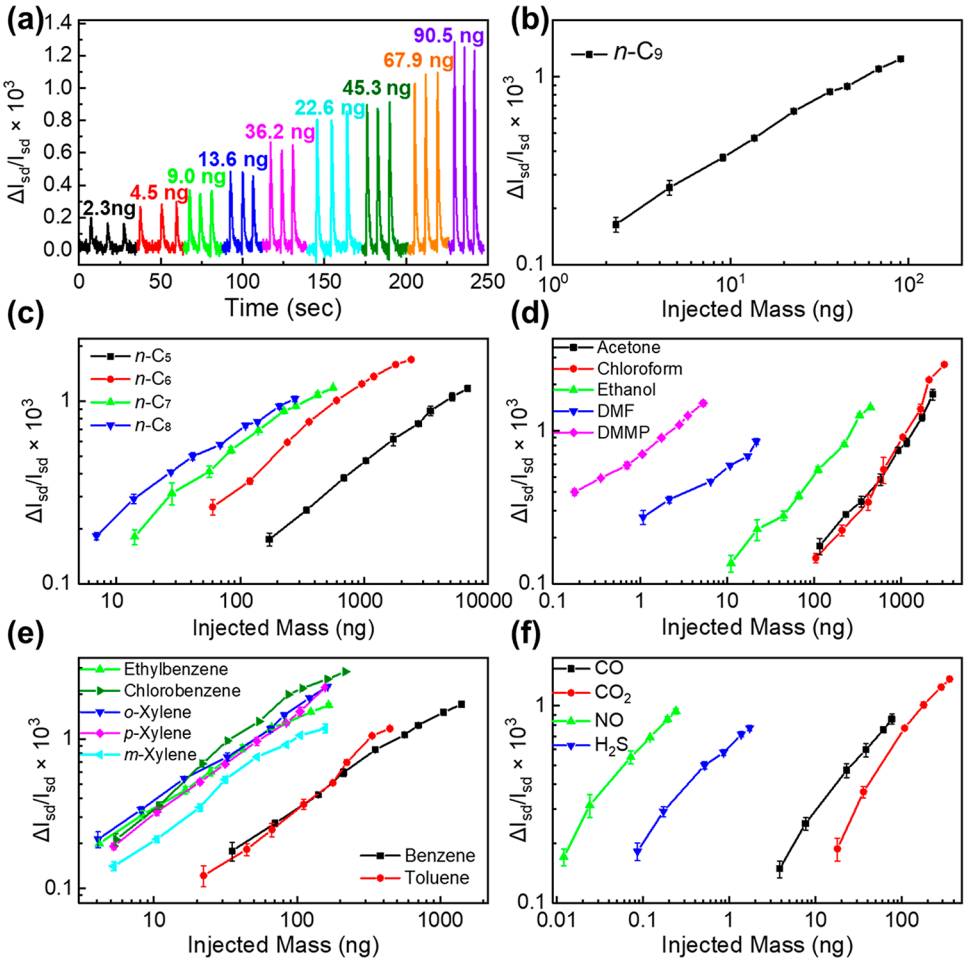

Figure 2. μColumn graphene sensor's responses to different chemical species. (a) Response of the sensor to repeated pulses of *n*-nonane injection with different masses as noted in the figure. The corresponding LOD at 3σ noise floor is estimated to be 2.1 ng. (b–f) Response of the sensor to *n*-nonane (b), alkanes (c), polar molecules (d), aromatic molecules (e), and inorganic analytes (f) of different masses in log–log scale.

changes occur when surface molecules alter the local dielectric environment above the graphene channel, which pulls more charges from the metal contacts. Consequently, the molecular fringing gate effect increases the transconductance of the FET by coupling with its back gate voltage. Importantly, instead of being measured directly through impedance spectroscopy, which is usually less sensitive and requires more complicated AC circuitry, this fringing capacitance change (C_{mol}) is first amplified *in situ* by graphene's high mobility (as shown in eq 3) and then measured conveniently as a DC current change. A unique microfabricated flow column (μColumn) for gas flow is integrated onto the graphene sensor to further enhance the interaction between the analytes and the sensor. Rapid (down to subseconds) and sensitive (down to parts-per-billion) label-free detection of a broad spectrum of vapor analytes, including 13 polar (10 organic and 3 inorganic) and 8 nonpolar (7 organic and 1 inorganic) molecules, was achieved on a centimeter-sized graphene FET (Gr-FET) integrated with a 40 cm long serpentine shaped μColumn.

Figure 1b illustrates the device geometry and measurement setup. The sensor chip consists of two parts, a 2 cm × 2 cm Gr-FET and a 40 cm long μColumn. Gr-FETs were fabricated using chemical vapor deposition (CVD)-grown graphene on a silicon wafer with thermal oxide (275 nm thick) and atomic layer deposition (ALD) deposited aluminum oxide (50 nm thick) for better gate electrical insulation. Two layers of graphene were transferred to guarantee coverage of graphene in the FET channel area. Next, the Gr-FET was capped with a 40 cm (length) × 400 μm (width) × 375 μm (depth) μColumn. The bonding of the μColumn and the Gr-FET was designed such that the metal contacts were covered, and only the graphene channel was exposed to the analytes. Details of device fabrication flow are discussed in the Supporting Information.

The as-obtained sensor was connected to a benchtop gas chromatography (GC) system that provides subsecond pulsed injection of analytes (see Methods in Supporting Information). The sensor was then exposed to known amount of analytes, while changes in the source-drain current (I_{sd}) were recorded with V_g kept at zero. The sensing response was calculated as the ratio of the transient current change to the baseline current ($\Delta I_{sd}/I_{sd}$). Initial results demonstrated that the sensor showed sharp and strong responses to all tested chemicals, ranging from nonpolar and weak polar to strong polar molecules. Figure 1c lists the DC current response of a typical μColumn graphene sensor to 21 representative chemical species, including normal alkanes (C_5–C_9), benzene, toluene, ethylbenzene, xylenes (*o*-, *m*-, and *p*-), 1,2-dichlorobenzene, acetone, chloroform, ethanol, *N*,*N*-dimethylformamide (DMF), dimethyl methylphosphonate (DMMP), carbon monoxide, carbon dioxide, nitric oxide, and hydrogen sulfide. All tested devices show instantaneous subsecond response

https://doi.org/10.1021/acs.nanolett.1c03416
Nano Lett. 2021, 21, 10301–10308

Table 1. Summary of the μColumn Gr-FET Sensor in Response to 21 Polar and Non-polar Vapor Analytes as well as Their 8 h Total Weight Average (TWA) Permissible Exposure Limits (PEWs) Listed by Occupational Safety and Health Administration (OSHA)

analyte	LOD, mass (ng)	concentration at detection limit mass (ppm)	$t_{1/2}$ (s)	OSHA PEL 8 h TWA (ppm)
n-C_5	128.5	162	0.6	1000
n-C_6	19.7	56.3	1.3	500
n-C_7	8.0	13.6	1.4	500
n-C_8	4.1	4.3	1.5	500
n-C_9	2.1	1.7	1.1	-
benzene	24.4	46.2	1	1
toluene	39.3	37.0	0.7	200
ethylbenzene	2.2	5.1	0.8	100
o-xylene	3.7	2.2	1.7	100
m-xylene	4.6	4.0	1.3	100
p-xylene	4.2	3.7	1.6	100
chlorobenzene	1.7	4.9	0.9	75
acetone	43.5	235.1	0.8	500
chloroform	33.3	149.4	0.6	100
ethanol	20.5	19.9	1.1	1000
DMF	0.43	0.7	1.6	50
DMMP	0.050	0.02	2.0	-
carbon monoxide	3.5	20.0	0.7	35
carbon dioxide	18	57.4	0.6	5000
nitric oxide	0.1	0.6	1.1	25
hydrogen sulfide	0.8	4.2	0.9	10

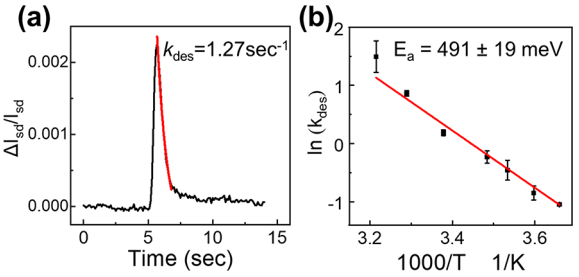

Figure 4. μColumn graphene sensor as a testbed for probing alkane–graphene binding energy. (a) μColumn graphene sensor's temporal response to pentane at 22.9 °C. Exponential fit in red to the desorption part yields the desorption rate k_{des} = 1.27 s^{-1} (τ_{des} = 0.79 s). (b) Desorption rates in the natural log scale plotted against the corresponding measurement temperatures in an Arrhenius plot, with the slope of the linear fit in red giving the binding energy E_a of 491 meV. The measurement temperatures here are 0.1, 4.9, 9.8, 13.9, 22.9, 30.8, and 37.7 °C, respectively.

Table 2. Summary of the Experimental Binding Energies, Dipole Moments, and Polarizabilities of Five Tested Alkanes[42]

analyte	dipole moment (D)	polarizability (α, 10^{-24} cm^{-3})	experimental binding energy (meV)
n-C_5	0	9.88	491 ± 19
n-C_6	0	11.63	527 ± 15
n-C_7	0	13.37	607 ± 30
n-C_8	0	15.24	684 ± 26
n-C_9	0	17.37	761 ± 30

when exposed to pulsed analytes (*i.e.*, Figure 1d for heptane). Furthermore, the sensor was completely regenerated (*i.e.*, the signal returned to baseline) without any post-treatment.

Next, to evaluate the μColumn graphene sensor sensing performance, its temporal responses to transient exposure to analytes with varying masses were recorded. The sensor responses (*i.e.*, $\Delta I_{sd}/I_{sd}$) to three repeated doses of *n*-C_9 with an injection mass from 2.3 ng to 90.5 ng are plotted in Figure 2a. To estimate the detection limit, sensor dosage response average is plotted in log–log scale (Figure 2b). The sublinear response reflects the transient behavior of vapor pulses interacting with the graphene surface and is consistent with previous observations from with other optical sensors[32] and our heterodyne graphene sensor.[28] Using a 3σ noise floor (3σ = 0.016 μA, Figure S2), the limit of detection (LOD) for *n*-C_9

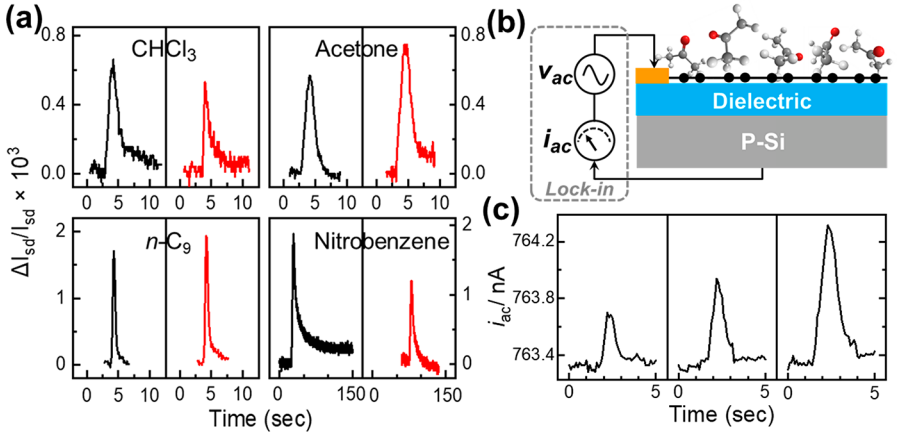

Figure 3. Fringing capacitive gating based sensing mechanism. (a) μColumn graphene sensor's response to chloroform, acetone, *n*-nonane, and nitrobenzene when gated at the p-branch (black) and the n-branch (red). For a given chemical species, the same mass of analyte was injected to the same device with gate bias set in the p- and n-branches, respectively. (b) Illustration of impedance measurement, where the device is configured as a "parallel capacitor" instead of a three-terminal transistor. The graphene together with the metal contact forms one plate, and the underlying p-doped silicon forms the other plate. The impedance was measured by applying AC voltage to the doped Si while both source and drain contacts are grounded. The AC current i_{AC} flowing through this capacitor was recorded with a lock-in amplifier. (c) i_{AC} response of the "parallel capacitor" to acetone injection with different mass amounts (from left to right: 1317 ng, 2633 ng, and 3950 ng).

https://doi.org/10.1021/acs.nanolett.1c03416
Nano Lett. 2021, 21, 10301–10308

Table 3. Performance Metrics of Various Electronic Sensor Technologies Compared to Those of the μColumn Graphene Sensor (the Ranges Are Estimated)

	chemiresistive sensor[23,43,44]	chemicapacitance sensor[19,45,46]	thermal conductivity detector[47−49]	nanowire/CNT/2D FET sensor[7,50,51]	μColumn graphene sensor (this work)
sensitivity	medium (ppm)	medium (sub-ppm to ppm)	medium (ppm)	very high (ppb to ppt)	high (sub-ppm to ppb, 10s of picograms to 10s of nanograms)
speed for response and regeneration	slow (10s of seconds to hours)	slow (10s of seconds to hours)	fast (<1 s)	slow (10s of seconds to hours)	fast (<1 s)
universal responsivity	partial	partial	yes	no	yes (polar, nonpolar, organic, and inorganic)
chemical treatment	often required	yes	no	often required	no
power consumption	low (10s to 100s of microwatts)	low (10s to 100s of microwatts)	high (sub-watt to watt)	low (10s to 100s of microwatts)	low (10s to 100s of microwatts, depending on the applied bias)

is estimated to be 2.1 ng (or 1.7 ppm by volume) at an S/N of 3.

To demonstrate the versatility of our μColumn graphene vapor sensor, we characterized the sensor's repeated dosage response to an additional 20 analytes, including four other alkanes from *n*-C_6 to *n*-C_9 (Figure 2c), seven aromatics (Figure 2d), four other organic polar molecules (Figure 2e), and four inorganic compounds (Figure 2f). Table 1 summarizes the extracted LOD in both mass and volume concentrations for all 21 analytes, together with full width at half maxima ($t_{1/2}$) at minimum injection amounts and corresponding OSHA standard for 8 h total weight-average (TWA) permissible exposure limits (PELs). In particular, the LOD for DMMP (Figure 2d) is estimated to be ∼0.050 ng (0.02 ppm in concentration), which represents an improvement of several orders of magnitude over most existing DC-based nanoelectronic sensors.[13,16,20,22,23,33] Critically, the μColumn graphene sensor is not only capable of detecting most common hazardous air pollutants (*e.g.*, benzene, toluene, ethylbenzene, and xylenes) but also achieves sensitivities exceeding the OSHA requirement for long-term exposure limits for nearly all 21 analytes. Therefore, these initial results already demonstrate its great potential for practical applications in real-time industrial safety monitoring.

The sensing mechanism for μColumn graphene sensors can be explained as follows. The change in carrier density in the graphene channel can be induced by either direct charge transfer between graphene and the adsorbate or fringing capacitive gating, in which the analyte changes the local permittivity. In the first case, depending on whether the analyte molecule is an electron donor or acceptor compared to graphene, the sensor current can show a positive or negative peak. Furthermore, due to the intrinsic ambipolarity of graphene, the dominant charge carrier can be either hole at negative V_g (with respect to the Dirac point or charge neutral point) or electron at positive V_g. Therefore, if charge transfer were the governing mechanism for the sensor current change, some analytes would show positive signals while others would show negative signals. Furthermore, the sensor signal would flip the sign when V_g is held on the opposite side of the Dirac point. As discussed previously, we have tested a total of 21 analytes on 20 devices. All results consistently show positive signals regardless of the analyte being an electron donor or acceptor. Furthermore, gate-dependent measurements for all tested analytes show a positive signal on both sides of the Dirac point, as exemplified in Figure 3a with chloroform, acetone, *n*-nonane, and nitrobenzene, which is a strong electron acceptor compared to graphene. These results rule out charge transfer to be the dominant mechanism in the present work.

We further explored the fringing capacitive gating effect as the main mechanism for our sensing results. In the case of capacitive gating, the graphene charge carrier density is changed not by direct charge transfer but by increasing the total gate capacitance when analyte molecules bind to the graphene surface. To confirm this capacitance-effect mechanism, direct two-terminal impedance measurements were conducted between the graphene channel and doped silicon bottom gate (Figure 3b). Herein, the device was treated as a parallel-plate capacitor instead of a three-terminal transistor: the graphene channel together with the metal contacts serves as one plate of the capacitor, with the other plate formed by the heavily doped Si substrate. The time-dependent impedance change is measured after analyte injection using a lock-in amplifier by applying a 95.57 Hz, 0.04 V AC voltage (v_{AC}) across the capacitor. As exemplified in Figure 3c, a significant increase in the AC current was observed after acetone injection. The response increases with increasing acetone mass. Since the parasitic impedance from the measurement setup and the sensor device remain constant during measurement, the increase in the AC current across the two parallel plates can only be explained by the enhanced device capacitance, which is induced by the injected analytes. This result provides direct evidence for the proposed fringing capacitance change based sensing mechanism. Notably, the injection amount had to be nine times higher in Figure 3c than in Figure 2 in order to achieve a similar S/N, highlighting the benefit of intrinsic amplification from the Gr-FET in Figure 2.

Next, we measured the sensor responses to three pairs of isomers, (1) *cis*- and *trans*-dicholoethylene, (2) 1,2- and 1,3-dichlorobenzene, and (3) 3- and 2-chlorotoluene. Although each pair of isomers has the same chemical constitution, differences in the dipole moment and hence polarizability result in different dielectric constants at the same vapor concentrations, as given by the Claussius−Mossoti equation.[34] For each pair of isomers, even with the same injection mass, the same sensor shows a significantly different sensitivity (Figure S3), which is roughly proportional to the corresponding dielectric constant (Table S1).

The above three control experiments—V_g-dependent sensing measurements (at n- and p-branches of Gr-FET), impedance measurements, and isomer measurements, collectively confirm that the fringing capacitive effect, instead of the charge transfer, is the dominant sensing mechanism in our sensor. Assuming negligible direct charge transfer between graphene and adsorbed molecules, C_{mol} is solely responsible for the current perturbation after analyte injection. C_{mol} and molecule induced charge perturbation Q_{mol} can be estimated as follows,

https://doi.org/10.1021/acs.nanolett.1c03416
Nano Lett. 2021, 21, 10301−10308

$$C_{mol} = C_g \cdot \frac{\Delta I_{sd}}{I_{sd}} \quad (4)$$

$$Q_{mol} = C_{mol} \cdot \left(V_g - V_{th} - \frac{1}{2}V_{sd}\right) \quad (5)$$

Table S2 summarizes the estimated C_{mol} and Q_{mol} of 21 analytes at the minimal injection amount, together with dipole moment and polarizability.

We also investigated the role of the μColumn. μColumns with different shapes and dimensions were designed as controls (Table S3), namely, with the same width and depth but a much shorter length of 11.8 cm (Figures S4b and S5), and rectangular shape with the same total area but much shorter in length and wider in width than the prototype μColumn (Figures S4c and S6). Control 1 has a lower sensitivity due to the smaller sensing area, which can also be seen in Figure S7 where the graphene channel area was further reduced from a centimeter scale to 2 μm × 2 μm. Control 2 has a lower sensitivity because it has a very wide channel. Given the high volumetric rate (8.5 mL/min) in our experiments, the molecules do not have enough time to fully interact with the graphene surface if the channel is too wide.

We also notice that for our prototype μColumn graphene sensor, the source−drain bias voltage plays an important role in sensitivity enhancement. When the bias was increased from 10 mV to 5 V, the signal-to-noise ratio (S/R) of the sensor increased from ∼1 to 27 (Figure S8). It is noticed that the conductance change toward injection of a given analyte with the same amount remains constant (Figure S8), and none of the detection peaks have any tailing issue; this is different from the previous DC sensing work,[33,35] where sensitivity shows significant dependence on V_{sd} and the signal does not emerge until above a threshold of applied voltage. In those works, the sensitivity and reversibility of the sensors were enhanced by a change in the charge transport mode, as in the Poole−Frenkel conduction regime electrons "jump" through the defects instead of bypassing them. In order to limit current going through the device, bias voltage of 3 V was adopted for all sensing performance characterizations in this work, which is sufficient to provide a decent S/N.

Unveiling the van der Waals (vdW) interactions between small molecules and sp^2 carbon allotropes is important for surface physics and sensor design, as well as in studying the related biological processes. Particularly, the behavior of rigid hydrocarbon chains on π systems is of special interest in organic synthesis, biochemistry, drug delivery, and hydrocarbon gas storage. To date, most studies are based on theoretical simulations[36,37] or thermal desorption spectroscopy measurements on graphite.[38−40] However, these methods might result in deviation of the molecular binding energies compared to those on graphene surfaces. A nanoelectronic chemical vapor sensor offers a more suitable platform to study the interactions between small molecules and the nanomaterials with their sensitive response and electrical readout.[1,3,4] However, as previously discussed, the response of conventional nanoelectronic sensors is based on charge transfer (covalent binding), which does not represent the physicochemical nature of noncovalent vdW interactions near the pristine surface of graphene. Using the heterodyne mixing detection technique, we have recently quantified the binding affinity between graphene and five polar molecule species.[29] However, the graphene heterodyne sensor is only responsive to polar molecules and unable to probe nonpolar molecules.

Unlike other graphene nanoelectronic sensors, the μColumn graphene sensor in the present work offers a testbed for characterizing the binding energy of adsorbed nonpolar molecules at the graphene surface. The high speed, high sensitivity, and reversible performance enables real-time monitoring of the rapid molecular physisorption behavior. Additionally, this sensor's design keeps both metal contacts and graphene edges outside the flow column, thus allowing the detection signal to unveil the true vdW interaction between the molecules and graphene.

To investigate the hydrocarbon/sp^2-carbon interaction, temperature-dependent measurements were conducted on the μColumn graphene sensor for five alkanes (from n-C_6 to n-C_9). The detailed testing method has been discussed in our previous paper.[29] Briefly, the device was kept on a Peltier cooler/heater to allow for device temperature control; for each analyte, time-domain measurements were conducted at different temperatures. The desorption rates are extracted at the first exponential decay of the curve (Figure 4a) and plotted against corresponding temperatures (Figure 4b). The binding affinity is then extracted by fitting the slope in Arrhenius scale, according to transition state theory.[41] The experimentally extracted binding energies of the four alkane chains on graphene are provided in Table 2. We notice that the binding energy between n-alkanes and graphene increases with increased chain length, in agreement with increased polarizability. These experimentally extracted values resemble the simulation results on graphene−alkane interactions.[36] However, compared to the modeling work on graphite, the corresponding binding energies of the same alkanes are lowered by ∼200 meV.[40]

In conclusion, we report a new nanoelectronic sensing mechanism by exploring the fringing capacitance change resulting from molecules binding to the graphene transistor surface. Unlike conventional impedance or capacitance sensing approaches, the dielectric response change is intrinsically amplified by the large transconductance of the graphene transistor and measured conveniently using DC readout. Our label-free μColumn DC graphene sensor demonstrates high speed, high sensitivity, and low power consumption and can detect a wide spectrum of analytes including polar/nonpolar and organic/inorganic molecules. The performance metrics of our μColumn graphene sensor in conjunction with other types of electronic sensors are summarized in Table 3. Furthermore, the μColumn design is compatible with existing μGC platforms, enabling the integration of this electronic sensor with μGC system for portable and wearable sensing applications.

■ ASSOCIATED CONTENT

Supporting Information

The Supporting Information is available free of charge at https://pubs.acs.org/doi/10.1021/acs.nanolett.1c03416.

Methods (device fabrication and measurement setup), addition experimental data, figures, and tables (PDF)

■ AUTHOR INFORMATION

Corresponding Authors

Xudong Fan − *Center for Wireless Integrated MicroSensing and Systems (WIMS2), University of Michigan, Ann Arbor,*

https://doi.org/10.1021/acs.nanolett.1c03416
Nano Lett. 2021, 21, 10301−10308

Michigan 48109, United States; Department of Biomedical Engineering, University of Michigan, Ann Arbor, Michigan 48109, United States; orcid.org/0000-0003-0149-1326; Email: xsfan@umich.edu

Zhaohui Zhong − *Department of Electrical Engineering and Computer Science, University of Michigan, Ann Arbor, Michigan 48109, United States; Center for Wireless Integrated MicroSensing and Systems (WIMS2), University of Michigan, Ann Arbor, Michigan 48109, United States;* orcid.org/0000-0001-5050-7182; Email: zzhong@umich.edu

Authors

Wenzhe Zang − *Department of Electrical Engineering and Computer Science, University of Michigan, Ann Arbor, Michigan 48109, United States; Center for Wireless Integrated MicroSensing and Systems (WIMS2), University of Michigan, Ann Arbor, Michigan 48109, United States;* orcid.org/0000-0003-2203-4634

Zhe Liu − *Department of Electrical Engineering and Computer Science, University of Michigan, Ann Arbor, Michigan 48109, United States*

Girish S. Kulkarni − *Center for Wireless Integrated MicroSensing and Systems (WIMS2), University of Michigan, Ann Arbor, Michigan 48109, United States; Department of Biomedical Engineering, University of Michigan, Ann Arbor, Michigan 48109, United States;* Present Address: Arborsense Inc., 1600 Huron Parkway, Ann Arbor, Michigan 48105, United States

Hongbo Zhu − *Center for Wireless Integrated MicroSensing and Systems (WIMS2), University of Michigan, Ann Arbor, Michigan 48109, United States; Department of Biomedical Engineering, University of Michigan, Ann Arbor, Michigan 48109, United States*

You Wu − *Department of Electrical Engineering and Computer Science, University of Michigan, Ann Arbor, Michigan 48109, United States*

Kyunghoon Lee − *Department of Electrical Engineering and Computer Science, University of Michigan, Ann Arbor, Michigan 48109, United States;* Present Address: Quantum Nanoelectronics Laboratory, Department of Physics, University of California at Berkeley, Berkeley, California 94720, United States, and Materials Sciences Division, Lawrence Berkeley National Laboratory, Berkeley, California 94720, United States; orcid.org/0000-0002-3409-9454

Maxwell Wei-Hao Li − *Center for Wireless Integrated MicroSensing and Systems (WIMS2), University of Michigan, Ann Arbor, Michigan 48109, United States; Department of Biomedical Engineering, University of Michigan, Ann Arbor, Michigan 48109, United States*

Complete contact information is available at: https://pubs.acs.org/10.1021/acs.nanolett.1c03416

Author Contributions

W.Z., Z.Z., and X.F. conceived the experiments. W.Z. and Z.L. fabricated the devices, developed the electrical measurement setup, and performed the measurements. G.S.K., Y.W., and K.L. provided support for fabrication and electrical measurement setup. H.Z. and M.W.-H.L. contributed to calibration of the GC system. All authors analyzed the data and cowrote the paper.

Notes

The views and conclusions contained herein are those of the authors and should not be interpreted as necessarily representing the official policies or endorsements, either expressed or implied, of the ODNI, IARPA, or the U.S. Government. The U.S. Government is authorized to reproduce and distribute reprints for Governmental purposes notwithstanding any copyright annotation thereon.
The authors declare no competing financial interest.

■ ACKNOWLEDGMENTS

This work was supported by the Office of the Director of National Intelligence (ODNI), Intelligence Advanced Research Projects Activity (IARPA), via IARPA 2018-18032000001. Devices were fabricated in the Lurie Nanofabrication Facility at the University of Michigan, a member of the NSF National Nanotechnology Infrastructure Network.

■ REFERENCES

(1) Lu, W.; Lieber, C. M. Nanoelectronics from the bottom up. *Nat. Mater.* **2007**, *6*, 841−850.
(2) Zhang, A.; Lieber, C. M. Nano-Bioelectronics. *Chem. Rev.* **2016**, *116*, 215−257.
(3) Geim, A. K.; Novoselov, K. S. The rise of graphene. *Nat. Mater.* **2007**, *6*, 183−191.
(4) McEuen, P. L.; Fuhrer, M. S.; Park, H. Single-walled carbon nanotube electronics. *IEEE Trans. Nanotechnol.* **2002**, *1*, 78−85.
(5) Wang, Q. H.; Kalantar-Zadeh, K.; Kis, A.; Coleman, J. N.; Strano, M. S. Electronics and optoelectronics of two-dimensional transition metal dichalcogenides. *Nat. Nanotechnol.* **2012**, *7*, 699−712.
(6) Giraldo, J. P.; Wu, H.; Newkirk, G. M.; Kruss, S. Nanobiotechnology approaches for engineering smart plant sensors. *Nat. Nanotechnol.* **2019**, *14*, 541−553.
(7) Anichini, C.; et al. Chemical sensing with 2D materials. *Chem. Soc. Rev.* **2018**, *47*, 4860−4908.
(8) Hu, H.; Yang, X.; Guo, X.; Khaliji, K.; Biswas, S. R.; Garcia de Abajo, F. J.; Low, T.; Sun, Z.; Dai, Q.; et al. Gas identification with graphene plasmons. *Nat. Commun.* **2019**, *10*, 1131.
(9) Shao, Y.; et al. Graphene based electrochemical sensors and biosensors: A review. *Electroanalysis* **2010**, *22*, 1027−1036.
(10) Stern, E.; et al. Label-free immunodetection with CMOS-compatible semiconducting nanowires. *Nature* **2007**, *445*, 519−522.
(11) Kong, J.; Dai, H. Full and modulated chemical gating of individual carbon nanotubes by organic amine compounds. *J. Phys. Chem. B* **2001**, *105*, 2890−2893.
(12) Schedin, F.; et al. Detection of individual gas molecules adsorbed on graphene. *Nat. Mater.* **2007**, *6*, 652−655.
(13) Rumyantsev, S.; Liu, G.; Shur, M. S.; Potyrailo, R. A.; Balandin, A. A. Selective gas sensing with a single pristine graphene transistor. *Nano Lett.* **2012**, *12*, 2294−2298.
(14) Perkins, F. K.; et al. Chemical vapor sensing with monolayer MoS2. *Nano Lett.* **2013**, *13*, 668−673.
(15) Kou, L.; Frauenheim, T.; Chen, C. Phosphorene as a superior gas sensor: Selective adsorption and distinct i - V response. *J. Phys. Chem. Lett.* **2014**, *5*, 2675−2681.
(16) Kumar, B.; et al. The role of external defects in chemical sensing of graphene field-effect transistors. *Nano Lett.* **2013**, *13*, 1962−1968.
(17) Star, A.; Han, T. R.; Gabriel, J. C. P.; Bradley, K.; Grüner, G. Interaction of Aromatic Compounds with Carbon Nanotubes: Correlation to the Hammett Parameter of the Substituent and Measured Carbon Nanotube FET Response. *Nano Lett.* **2003**, *3*, 1421−1423.
(18) Star, A.; Han, T. R.; Joshi, V.; Gabriel, J. C. P.; Grüner, G. Nanoelectronic carbon dioxide sensors. *Adv. Mater.* **2004**, *16*, 2049−2052.

(19) Snow, E. S.; Perkins, F. K.; Houser, E. J.; Badescu, S. C.; Reinecke, T. L. Chemical detection with a single-walled carbon nanotube capacitor. *Science* **2005**, *307*, 1942−1945.
(20) Kauffman, D. R.; Star, A. Carbon nanotube gas and vapor sensors. *Angew. Chem., Int. Ed.* **2008**, *47*, 6550−6570.
(21) Lee, C. Y.; Sharma, R.; Radadia, A. D.; Masel, R. I.; Strano, M. S. On-chip micro gas chromatograph enabled by a noncovalently functionalized single-walled carbon nanotube sensor array. *Angew. Chem., Int. Ed.* **2008**, *47*, 5018−5021.
(22) Li, J.; et al. Carbon nanotube sensors for gas and organic vapor detection. *Nano Lett.* **2003**, *3*, 929−933.
(23) Dua, V.; et al. All-organic vapor sensor using inkjet-printed reduced graphene oxide. *Angew. Chem., Int. Ed.* **2010**, *49*, 2154−2157.
(24) Bergstrom, P. L. *A microfabricated work-function gas sensor for semiconductor process gas detection*; University of Michigan: 1996.
(25) Madou, M. J.; Cubicciotti, R. Scaling issues in chemical and biological sensors. *Proc. IEEE* **2003**, *91*, 830−838.
(26) Kulkarni, G. S.; Zhong, Z. Detection beyond the Debye screening length in a high-frequency nanoelectronic biosensor. *Nano Lett.* **2012**, *12*, 719−723.
(27) Kulkarni, G. S.; Zhong, Z. Fabrication of carbon nanotube high-frequency nanoelectronic biosensor for sensing in high ionic strength solutions. *J. Vis. Exp.* **2013**, 50438.
(28) Kulkarni, G. S.; Reddy, K.; Zhong, Z.; Fan, X. Graphene nanoelectronic heterodyne sensor for rapid and sensitive vapour detection. *Nat. Commun.* **2014**, *5*, 4376.
(29) Kulkarni, G. S.; et al. Electrical Probing and Tuning of Molecular Physisorption on Graphene. *Nano Lett.* **2016**, *16*, 695−700.
(30) Kulkarni, G. S.; Zang, W.; Zhong, Z. Nanoelectronic Heterodyne Sensor: A New Electronic Sensing Paradigm. *Acc. Chem. Res.* **2016**, *49*, 2578−2586.
(31) Novoselov, K. S.; et al. Two-dimensional gas of massless Dirac fermions in graphene. *Nature* **2005**, *438*, 197−200.
(32) Reddy, K.; et al. Rapid, sensitive, and multiplexed on-chip optical sensors for micro-gas chromatography. *Lab Chip* **2012**, *12*, 901−905.
(33) Salehi-Khojin, A.; Field, C. R.; Yeom, J.; Masel, R. I. Sensitivity of nanotube chemical sensors at the onset of Poole-Frenkel conduction. *Appl. Phys. Lett.* **2010**, *96*, 163110.
(34) Jackson, J. D. *Classical Electrodynamics*, 3rd ed.; John Wiley & Sons, Inc.: 1998.
(35) Salehi-Khojin, A.; Lin, K. Y.; Field, C. R.; Masel, R. I. Nonthermal current-stimulated desorption of gases from carbon nanotubes. *Science* **2010**, *329*, 1327−1330.
(36) Londero, E.; et al. Desorption of n-alkanes from graphene: A van der Waals density functional study. *J. Phys.: Condens. Matter* **2012**, *24*, 424212.
(37) Yang, J. S.; Yang, C. L.; Wang, M. S.; Chen, B. D.; Ma, X. G. Crystallization of alkane melts induced by carbon nanotubes and graphene nanosheets: A molecular dynamics simulation study. *Phys. Chem. Chem. Phys.* **2011**, *13*, 15476−15482.
(38) Paserba, K. R.; Gellman, A. J. Effects of conformational isomerism on the desorption kinetics of n-alkanes from graphite. *J. Chem. Phys.* **2001**, *115*, 6737−6751.
(39) Paserba, K. R.; Gellman, A. J. Kinetics and energetics of oligomer desorption from surfaces. *Phys. Rev. Lett.* **2001**, *86*, 4338−4341.
(40) Gellman, A. J.; Paserba, K. R. Kinetics and mechanism of oligomer desorption from surfaces: n-alkanes on graphite. *J. Phys. Chem. B* **2002**, *106*, 13231−13241.
(41) Gabor, A. S. *Introduction to Surface Chemistry and Catalysis*; Wiley: New York, 1994.
(42) Rumble, J. R.; et al.. *CRC handbook of chemistry and physics*, 102nd ed.; CRC Press: 2021.
(43) Bohrer, F. I.; Covington, E.; Kurdak, Ç.; Zellers, E. T. Characterization of dense arrays of chemiresistor vapor sensors with submicrometer features and patterned nanoparticle interface layers. *Anal. Chem.* **2011**, *83*, 3687−3695.
(44) Liu, S. F.; Moh, L. C. H.; Swager, T. M. Single-walled carbon nanotube-metalloporphyrin chemiresistive gas sensor arrays for volatile organic compounds. *Chem. Mater.* **2015**, *27*, 3560−3563.
(45) Blue, R.; Uttamchandani, D. Chemicapacitors as a versatile platform for miniature gas and vapor sensors. *Meas. Sci. Technol.* **2017**, *28*, 022001.
(46) Patel, S. V.; et al. Chemicapacitive microsensors for volatile organic compound detection. *Sens. Actuators, B* **2003**, *96*, 541−553.
(47) Rastrello, F.; et al. Thermal conductivity detector for gas chromatography: Very wide gain range acquisition system and experimental measurements. *IEEE Trans. Instrum. Meas.* **2013**, *62*, 974−981.
(48) Narayanan, S.; Alfeeli, B.; Agah, M. Two-port static coated micro gas chromatography column with an embedded thermal conductivity detector. *IEEE Sens. J.* **2012**, *12*, 1893−1900.
(49) Kaanta, B. C.; Chen, H.; Zhang, X. A monolithically fabricated gas chromatography separation column with an integrated high sensitivity thermal conductivity detector. *J. Micromechanics Microengineering* **2010**, *20*, 055016.
(50) Kim, D. R.; Lee, C. H.; Zheng, X. Probing flow velocity with silicon nanowire sensors. *Nano Lett.* **2009**, *9*, 1984−1988.
(51) Schroeder, V.; Savagatrup, S.; He, M.; Lin, S.; Swager, T. M. Carbon nanotube chemical sensors. *Chem. Rev.* **2019**, *119*, 599−663.

https://doi.org/10.1021/acs.nanolett.1c03416
Nano Lett. 2021, 21, 10301−10308